Sensors and Actuators A 317 (2021) 112452

Contents lists available at ScienceDirect

Sensors and Actuators A: Physical

journal homepage: www.elsevier.com/locate/sna

# Flexible electrostatic transducer array with displacement control for haptic sensing and actuation

Ian Trase [a], Hong Z. Tan [b], Zi Chen [a], John X.J. Zhang [a,*]

[a] Thayer School of Engineering, Dartmouth College, 14 Engineering Drive, Hanover, NH 03755, USA
[b] School of Electrical and Computer Engineering at Purdue University, West Lafayette, IN 47907 USA

ARTICLE INFO

*Article history:*
Received 26 April 2020
Received in revised form
15 September 2020
Accepted 17 November 2020
Available online 23 November 2020

*Keywords:*
Haptics
Transducer
Electrostatic
Flexible electrodes
Sensing
Displacement control

ABSTRACT

We developed flexible electrostatic transducers with both a single element and a 2 × 2 array format to actuate at a precise displacement across a range of loads with a control circuitry and algorithm. The transducer, composed of a moving buckled film with an integrated electrode and a rigid electrode, can be used to simultaneously generate and sense displacements. A circuit and computer program were designed to demonstrate displacement control and quantify the sensing precision of the transducer. Specifically, we applied a range of voltage and load conditions to the transducer and array and measured the displacement while under loading through capacitive sensing. The change in capacitance was linear with respect to the area of the electrode in contact and matched theoretical predictions when described as a function of the displacement. The transducer was loaded with weights in the range of 5–27 mN and capacitance-driving voltage graphs were obtained. An 8 Hz driving frequency was used to move the transducer, while a 10.8 kHz signal was used to sense the capacitance. These were used to build a predictive model to correct for sensed load to maintain a average displacement. It was found that a transducer of dimensions 10 mm X 40 mm was able to maintain displacement under loads of 5–27 mN, while a matrix composed of 10 mm X 20 mm transducers was able to maintain displacement under loads of 2.5−11 mN. In general, the detection thresholds of human skin can range between 5–20 mN of force and 2–20 u m of displacement for frequencies between 1 Hz and 250 Hz, so these values are in line with what is needed to build a functional haptic wearable device. The present work provides a method to quantitatively measure and control a new type of flexible transducer for a variety of haptic applications.


## 1. Introduction

Transducers are used in both actuation and sensing applications, for example, as speakers and microphones [1], or for haptic wearable devices [2]. Many modern transducers are made from piezoelectric crystals such as lead-zirconium titanate (PZT) [3], which change shape in response to an applied voltage, or change voltage in response to an external force. These piezoelectric transducers can be made to be very precise and find use in small-scale control systems or measurement systems [4]. Another example of a common transducer would be the voice coil [5,6], which is composed of coiled wire. When an electrical current is passed through the wire, it generates a strong magnetic field to move a coil. This technology is common in speakers and microphones. However, most common transducers have several limitations which prevent their entry into new markets. Both ceramic piezoelectrics such as PZT and voice coils are rigid, and voice coils can have high energy requirements [7]. Piezoelectric polymers are a promising new field of research, with materials like polyvinylidene fluoride (PVDF) able to generate large displacements [8], but the polymers tend to have significantly lower piezoelectric constants than the ceramics [9]. This means that higher voltages and power outputs are necessary to generate the same level of displacement. Finally, most commercial transducers are restricted to either sensing or actuating, even if the fundamental material that drives them is capable of both (although see [10]). As modern technology becomes more integrated, there is a need for transducers capable of both sensing and actuation with the same element, even simultaneously. Typical applications include devices such as fitness wearables, smartwatches, or health-focused devices. Continuous sensing allows for higher quality data, especially when recording physiological signals. We have previously designed a flexible electrostatic transducer powerful enough to be used in haptics applications and show here that it is also capable of useful simultaneous sensing and actuation [11,12].

The flexible electrostatic actuator is composed of a moving buckled electroded film connected to a rigid electrode, as shown in

* Corresponding author.
*E-mail address:* john.zhang@dartmouth.edu (J.X.J. Zhang).

https://doi.org/10.1016/j.sna.2020.112452
0924-4247/

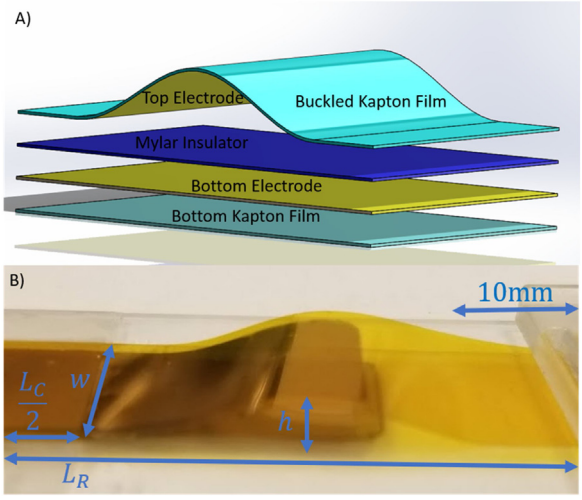


**Fig. 1.** Flexible electrostatic transducer. A) Schematic of transducer layers. B) Image of prototype transducer. As the applied voltage compresses the transducer, the capacitive area between the top and bottom Kapton films increases. This increases the overall capacitance by a precise amount and allows for the determination of displacement. A properly designed circuit can drive actuation while measuring the instantaneous capacitance change. When a load is applied, the transducer remains compressed at all stages, and the change in displacement $\Delta d$ is smaller.

Fig. 1a. Flexibility has previously been shown to be a crucial component in many soft actuator or conformal technologies [13–16]. When a voltage is applied between the two films, electrostatic force will pull the buckled film in towards the rigid film, similar to the action of electrostatic MEMS devices [17], but without the pull-in effect [18]. This allows the film to actuate and generate vibration when an AC voltage passes through it. As it is composed of a pair of electrodes, it is electrically similar to a parallel plate capacitor. The capacitance of the transducer changes significantly based on the degree to which it is displaced. Thus, by passing a high-frequency current through the transducer, the current shape and thus the displacement can be determined. While the transducers in most systems are designed to either sense or actuate, a benefit of the technology is that a standard device can do both, switching between actuation and sensing as the need arises. This is similar to how piezoelectric actuators work in ultrasonic imaging to first send and then receive an ultrasonic pulse [19]. Through careful design of the electronic and physical systems, these devices can sense and actuate simultaneously. This allows for smoother operation, better data collection, and higher-fidelity actuation output. If we can avoid interruptions in actuation caused when a device switches to a sensing mode, the user will feel an uninterrupted signal. Similarly, there will be no gaps in the sensed data. Simultaneous input and output allow for a further improvement to this class of devices – automatic displacement control. Self-sensing is a well understood process in piezoelectrics and dielectric elastomer actuators [20–22], but has not been extensively studied with flexible electrostatics. When sensing while actuating, the device can also sense its own motion. With the correct circuitry and programming, it can then adjust if the motion is too large or too small. This technique requires a good understanding of the electromechanical response of the transducers to different driving amplitudes, frequencies, and loads. In addition, whatever system is designed must be able to differentiate between motions generated by the electrostatic response of the transducer and motion external to the system.

The device is composed of a buckled 25$\mu$m Kapton film mounted to a rigid film composed of a Mylar insulator, a sputtered gold electrode, and a backing Kapton layer. Kapton was chosen for the buckled film due to its favorable electromechanical properties. Kapton has a high dielectric breakdown, allowing it to take high voltages despite its low thickness. It is also relatively stiff, which translates to an ability to generate higher forces when actuating. Specifically, the buckled film material and thickness was chosen to fall within a certain stiffness band, such that it was stiff enough to generate displacement into the skin, but not so stiff as to require very high voltages to move. The dimensions of the transducer were chosen to be $L_R = 20$mm, $w = 10$mm, and $h = 3$mm. These dimensions were chosen to optimize the displacement response at the voltage range under study. Simulations and theory were conducted during the design phase to ensure that the resulting device was capable of produce a perceptible signal into the skin, and the results of this research are presented in [23].

## 2. Theory

The haptic transducer device design is shown in Fig. 1. It consists of a fixed electroded film and a buckled electroded film, separated by a thin insulation layer. When a voltage is applied across the two electrodes, an electrostatic force is induced, and the two films move closer together. Generally, the electric field between the two electrodes is approximately zero everywhere they are not in contact, except for the small portions immediately adjacent to the contact area. These portions experience high fields and high acceleration, which pulls the immediate parts of the films together. This in turn brings the next infinitesimal segment of films together, and so on. Macroscopically, the end state of the device when charged to a given voltage is a function of the competition between the restorative bending energy of the buckled film and the electrostatic energy in the fields. By applying an alternating voltage, the buckled film can be made to move up and down and to vibrate. Unlike a standard parallel plate micro-electromechanical (MEMS) device, the transducer does not experience pull-in, as the bending energy of the buckled film increases more quickly at large deformations than the electrostatic energy. By changing the electrode patterning, the film can be made to actuate in a variety of ways, including up-and-down and side-to-side.

$$F_E = \frac{\varepsilon A V^2}{2d^2} \tag{1}$$

Here $\varepsilon$ is the permeability of the insulator, $A$ is the area of the two films that are in contact, $V$ is the applied driving voltage, and $d$ is the insulator thickness. The voltage necessary to reach a target displacement is dependent on the shape and size of the transducer, with larger and taller transducers requiring a higher voltage. The most important variable, however, is the thickness of the insulative film between the two electrodes. As the insulative film shrinks, the electric field becomes stronger at the same voltage, and less voltage is required to actuate the device. Theoretically, a 50 % decrease in film thickness would result in a 75 % decrease in required voltage for the same electric field strength, as shown in Eq. 1. There is a lower bound on insulator thickness that is given by the smoothness of the film and the dielectric breakdown strength – smoother and stronger films can be made thinner yet still function as effective insulators. Current devices are made with a Mylar insulate of either 12.5 or 2.5 $\mu$m. The properties of the insulator also strongly affect the capacitance of the device, which is critical for sensing.

Because the device is essentially a flexible capacitor, it can be used as a displacement sensor. When the distance between the buckled film and the rigid film decreases, the overall capacitance of the device increases. Specifically, the capacitance of the device is directly proportional to the amount of surface of the buckled film that is in contact with the rigid film. This relationship is described by Eq. (2). If one knows the capacitance of the device at rest and the capacitance when maximally compressed, it is straightforward to determine the expected capacitance at any point in between.

This allows the device to be used as a passive displacement sensor, with the real-time capacitance corresponding to the instantaneous displacement.

$$C = \frac{\varepsilon A}{d} = \frac{\varepsilon L_C w}{d},\ y(x) = \frac{h}{2}\left(1 - \cos\left(\frac{2\pi x}{L_R - L_C}\right)\right),$$
$$L_B - L_C = \int_0^{L_R - L_C} \sqrt{1 + \left(\frac{dy}{dx}\right)^2}\, dx \tag{2}$$

Here $C$ is the capacitance of the transducer, $w$ is the width of the transducer, $L_C$ is the length of the two films that are in contact, $L_B$ is the total length of the buckled film, $L_R$ is the total length of the rigid film, and $h$ is the height of the transducer. The capacitance can be found by solving for the relationship between $L_C$ and $h$. This is done by calculating the arc length of the buckled film that is not in contact with the rigid film and is instead buckled into a cosine shape $y(x)$. A complication arises when the transducer is under load as the transducer is more compressed, and hence its capacitance is higher at all points. In addition, the same amount of displacement results in a smaller change in capacitance. Looking at Eq. (2), this translates to the fact that the higher $L_C$ begins, the less it will change by when the voltage is turned on. A smaller change in $L_C$ leads to a smaller change in $C$, even if the change in $h$ is the same. If our goal is to simply measure displacement as a simple function of the capacitance, then any load will throw off that measurement completely. However, a given driving voltage will generate a specific capacitance as a function of the load. We can take this data, which is obtainable both through theory and experiments, and apply it to our sensing system. When the capacitance of the transducer is greater than it should be for a given driving voltage, we can calculate the load that must be applied, and from that load and the driving voltage estimate the displacement. Once this is done, it is possible to compensate with a precise increase in the driving voltage that will bring the displacement back to the target value. However, to perform real-time control, we must be able to sense and actuate at the same time.

Sensing and actuating simultaneously presents several engineering challenges. The displacement-frequency profile of the device is such that the driving frequencies must be less than 100 Hz, and often less than 50 Hz. However, the capacitance of the device is in the picofarad range, which requires higher frequencies to be sensed correctly. Furthermore, the driving signal must be of high voltage in order to generate perceptible actuation – in this device between 100–300 V peak-to-peak amplitude with zero DC offset. The circuitry required to measure the capacitance of the transducer is rated for normal electronics voltages, in the 1–15 V range. Exposing the capacitance measurement circuitry to the driving signal would cause the integrated circuits to immediately break down. The solution is to send a combined signal, with both the low and high frequency components, through the transducer, and to measure the capacitance on the low-voltage side of the transducer only. Because the capacitance of the device is low and the frequency of the high-voltage signal is also low, the vast majority of the low-frequency voltage drop occurs across the transducer, and only an extremely small low-frequency signal is present at the capacitance-sensing circuit. Conversely, a significant percentage of the low-voltage, high-frequency signal passes through the transducer. This percentage is controlled by the instantaneous capacitance of the transducer – by measuring the voltage drop of the high-frequency signal across a resistor and capacitor after the transducer, we can calculate the transducer capacitance. As long as the transducer does not suffer any sort of electrical breakdown, the vulnerable circuitry is never exposed to more than a few volts, the transducer receives the high voltage it needs to operate, and the circuit itself remains simple and robust.

The addition of a matrix presents another set of challenges. When each transducer on a matrix is addressed, driven, and controlled separately, each transducer can be treated like an individual system and the automatic sensing schema does not need to change. We chose to evaluate more complicated scenarios in which the transducers on the matrix were not electrically isolated from each other. Each top film was connected, and each rigid film was connected. Thus, when a driving signal was sent to the transducer matrix, all transducers actuated at the same amplitude, frequency, and phase. Under this setup, when a mechanical load is placed on a transducer, the overall change in capacitance will be only 25 % of what it would have been with a single transducer. By focusing on a single transducer in the matrix, it is possible to prescribe the displacement for that transducer while letting the other transducers operate without loads.

## 3. Fabrication and experimental setup

The transducer itself is composed of a pair of thin films mounted on a glass slide. We use a 25$\mu$m –thick Kapton film for the buckled film, as it has a high dielectric breakdown strength and is relatively stiff, which leads to higher forces. A thin coat of 20 nm of gold is sputter-coated onto this film in a precise pattern, and a wire is attached using copper tape. The rigid film is composed of a thick layer of PDMS ($\sim$100$\mu$m) onto which another 20 nm of gold is patterned on. Another wire and copper tape are placed on this gold electrode. After the gold is sputtered onto the PDMS, an extremely thin freestanding sheet of Mylar film (2.5$\mu$m) is affixed to the PDMS-gold surface. The PDMS acts as an adhesive and allows the Mylar to stay flat. Mylar is an excellent insulator and allows there to be a 2.5$\mu$m separation between the two gold electrodes, leading to high electric fields and forces. Finally, the Kapton film is buckled to give a predetermined maximum height and fixed to the rigid film.

The experimental setup consisted of a series of electronics designed to amplify and modulate the desired signals. The circuit is described in detail in Fig. 2b. The driving signal output was generated using the audio port of a desktop computer and was controlled through a custom MATLAB script. The audio port was capable of generating a signal of between 1 Hz-24 kHz, and a voltage amplitude of up to 2 $V_{p2p}$. This signal was then passed through a Texas Instruments LM1458 N op-amp amplifying circuit to bring the maximum amplitude to 10 $V_{p2p}$, which allows us to access the full range of the high voltage amplifier. In general, the amplitude was set to between 10–30 $V_{p2p}$. This signal was then added to a 300m$V_{p2p}$ 10.08 kHz signal generated by a Keysight 33522B signal generator using a summing op-amp configuration, as shown in Fig. 2b. The combined signal was then passed to the Trek Model 2210 high-voltage amplifier with a gain of 100. Thus, the final signal as output from the high-voltage amplifier was a 100–300 $V_{p2p}$ amplitude signal of low frequency summed with a 30 $V_{p2p}$ amplitude 10.08 kHz signal. This signal was passed through the transducer and then passed through a sensing resistor. The resistance of this resistor was chosen to be 10k$\Omega$ such that the voltage amplitude across it would not exceed 1 V under maximum actuation parameters (100 Hz driving frequency, 300 $V_{p2p}$ driving amplitude, max transducer capacitance 50pF). A probe connected to a National Instruments DAQ measured the voltage drop across the chosen resistor and delivered that data to the running MATLAB script.

The MATLAB program consisted of three parts: a method to generate and output the audio signal used to drive the transducer motion; a method to read the measured voltage drop across the resistor which corresponded to the capacitance of the transducer; and a method to use the transducer capacitance, the audio signal amplitude, and the target displacement to both measure the load on the transducer and ensure a average displacement amplitude.

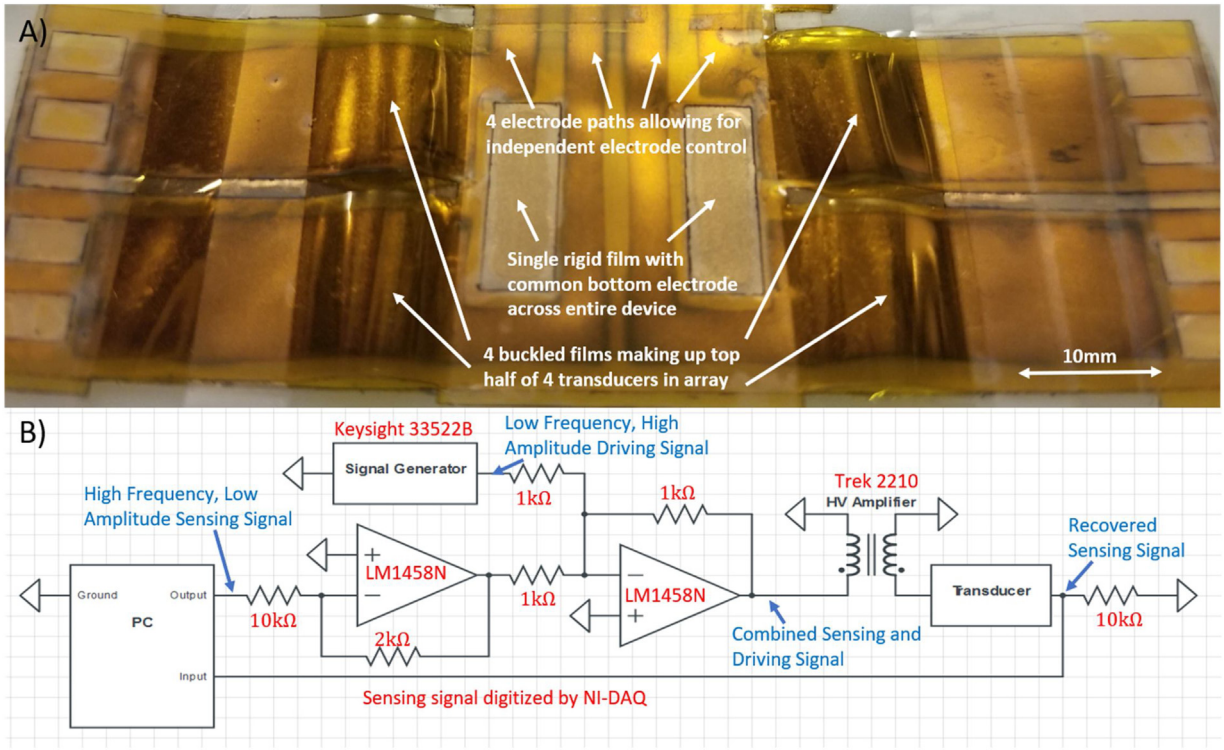


**Fig. 2.** Electronic Setup. A) Transducer array, showing the buckled film with four separate laser cut transducers and sputtered electrodes, and a single shared ground on the rigid electrode. Measurements were conducted on a single transducer on the array, to compare results between an array transducer and a solo transducer. B) circuit diagram, describing basic layout of control system, with associated driving and sensing signals.

Audio signals could be generated at any frequency the audio jack was capable of outputting, and the signals could be set to run continuously or for a discrete period of time. The measurement method could be called to collect voltage data for any length of time at a maximum rate of 102,400 samples per second. The audio signal and measurement method could be started simultaneously, making it possible to measure phase delay and track motion in real-time.

The MATLAB program was designed to adjust the voltage being sent to the device in response to a change in the capacitance. When given a target displacement, the program would first send a fixed driving voltage through the transducer and measure the maximum and minimum capacitances, and then use calibration data to determine the load on the transducer. Once the load is known, the program was able to choose a target driving voltage to reach the specified displacement.

The basic construction of the transducer matrix was similar to the single transducer. An Anatech Hummer was used to sputter-coat the rigid film with a single large gold electrode, while the buckled film was patterned with four separate electrodes. In this system, all four transducers share a common ground but can be actuated at different voltages and frequencies if desired. It was important that all four transducers shared a similar geometry, such that the same driving signal sent to two transducers would generate the same motion in both. To this end, the buckled Kapton film was laser-cut using a custom pattern, and then sputtered using another custom mask. These patterns were designed to maximize lamination between the buckled and rigid films while still allowing for wire pathing and uniform geometry. The results of this fabrication can be seen in Fig. 2A.

## 4. Results and discussion

The transducer was tested under a variety of loading, driving, and target displacement conditions. The goals of these tests were twofold. Firstly, we wanted to show that the transducer was capable of measuring the load placed on it while actuating. Secondly, that the transducer could maintain a average displacement for a range of loading conditions without external input. In Fig. 3, we show the results of the load measurement test. Loads from 1 mN to 9 mN were placed on the centerpoint of the buckled film of the transducer using a flexible lightweight bucket of folded paper to prevent loads from falling to one side or another, and the capacitance of the transducer was measured as a function of the driving amplitude at 8 Hz. The bucket was attached using a thin strip of tape and was designed to minimize any potential increase in transducer stiffness. In Fig. 3a, we can see that there is a linear increase in capacitance as the load is increased for any driving voltage. We also conduct a load measurement test for the transducer matrix by applying loads to only one of the four transducers, and then measuring the resulting total capacitance. As the displacement on the other three transducers is unaffected by the load, this reduces the ultimate sensitivity of the capacitance measurement by 25 %. Despite this, we see the same trends in terms of minimum and maximum capacitance as voltage increases. The different fabrication methods between the single transducer and the transducer matrix result in different capacitance ranges and different voltage ranges, but the overall structure of the phenomena remains the same.

The calculated capacitance can be related to the exact position of the transducer through Eq. (2). Because a large change in $L_C$ corresponds to only a small change in the height $h$, the relationship between $L_C$ and $h$ is almost entirely linear, and thus the change in capacitance $\Delta C$ between the minimum and maximum values is proportional to the change in height, regardless of the base capacitance (and base compression of the transducer). For any driving voltage, we can immediately determine both the load and the current displacement by measuring the change in capacitance and baseline capacitance, then correlating it to the data in Fig. 3. With this information, we can calculate what driving voltage would be

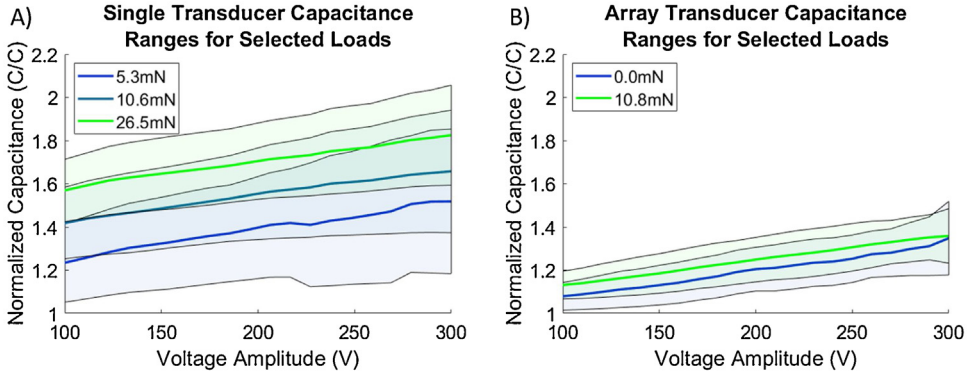


**Fig. 3.** Capacitance vs. driving voltage for selected loading conditions. Each color represents a specific loading condition, such that the transducer is loaded with 5.3 mN in the blue curve in A). As the transducer actuates, its capacitance increases and decreases in time with the driving frequency (8 Hz), producing a minimum and maximum capacitance value at each driving voltage amplitude. These minimum and maximum capacitances are represented by the bottom and top of the shaded region, respectively, with the average capacitance at each driving voltage value plotted directly. Heavier loads tend to produce larger average capacitances, while higher driving voltages increase the spread between minimum and maximum capacitance. Capacitance values are normalized with respect to the minimum measured capacitance at 50 V, as the percentage change in capacitance is the metric used to measure the loads and calculate displacements. A) Capacitance data for single transducer. B) Capacitance data for a transducer on the array.

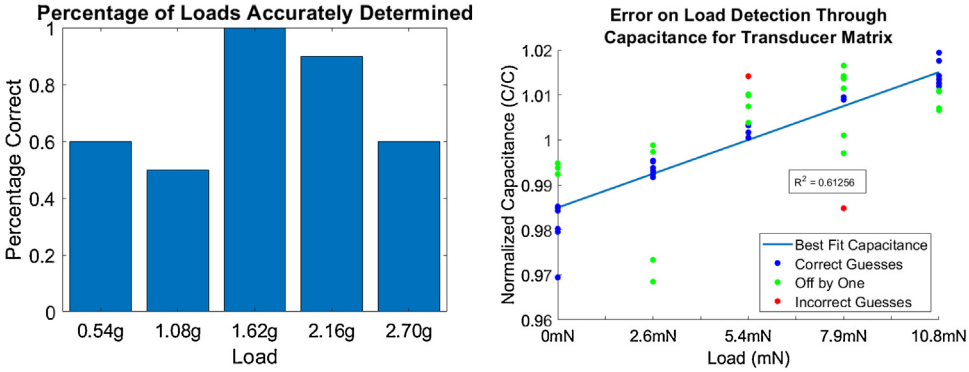


**Fig. 4.** A) Percentage of loads accurately determined by the transducer. B) Error on load detection for the transducer matrix.

necessary to generate the target displacement, which is equivalent to a target change in capacitance, under this particular load and increase the driving voltage to this value.

In order to accurately control the displacement of the transducer, it is important to be able to detect the amount of force being applied to the transducer. This can be done using the data collected in Fig. 3, by measuring the baseline capacitance of the transducer at a particular driving voltage and correlating it to a given load. In Fig. 4, a series of 50 trials were conducted, wherein a random load was applied, and then the system would attempt to detect the load based on the capacitance of the transducer. The five weights from Fig. 3 were used, and trials were marked as either a success or failure based on whether the correct load was identified, shown in Fig. 4(A). For the transducer matrix, a different system was used to account for the fact that a load was only placed on one of the four transducers while the capacitance was measured from all of them. Here trials were marked as successes or failures based on their deviations from the best fit capacitance for the matrix. In all, in 24 of the 50 trials, the loads were accurately determined, in another 24 they were off by one load option, and the final 2 trials were off by multiple options. As sensitivity of the transducer matrix is significantly lower than that of the single transducer when operated in this mode, it was expected that the number of correct identifications would also be lower. The transducer matrix results show that the system remains reasonably accurate even under this more challenging scenario, which bodes well for future sensitivity improvements.

Lastly, an experiment was designed to explore the use of capacitance-based sensing to adjust the output displacement of the transducer. The goal of this experiment was to show that given a target displacement, the amplitude of the driving signal sent to the transducer could be adjusted such that the transducer was actuating at that target displacement, regardless of the load on the displacement. To do this, the measured capacitance range from the actuating transducer is first used to determine an approximate load. A target displacement is then translated into a target capacitance range using Eq. 2. Based on the target capacitance range and the estimated load, a new driving voltage is chosen using the calibration data described in Fig. 3. The resulting new change is capacitance is then recorded and translated back into a displacement value using Eq. 2, and this result is recorded.

50 measurement trials were conducted over 5 different loads and 10 different target capacitances (resulting in 50 unique target displacements). These results were collected into 5 groups of target displacements, to determine if the magnitude of displacement was a factor in error. Fig. 5 shows the results of these trials for the single transducer and transducer array in histograms with truncated y-axis. The overall control error can be calculated by dividing the absolute difference in the measured and target displacements by the total range of the target displacements. This yields an error of 9.5 % for the single transducer and 10.5 % for the transducer array. It is also useful to note that while the error was relatively constant with respect to displacement level for the single transducer, it was not for the transducer array. There are a few possible reasons for this, but the most likely is a mismatch between the assumed and

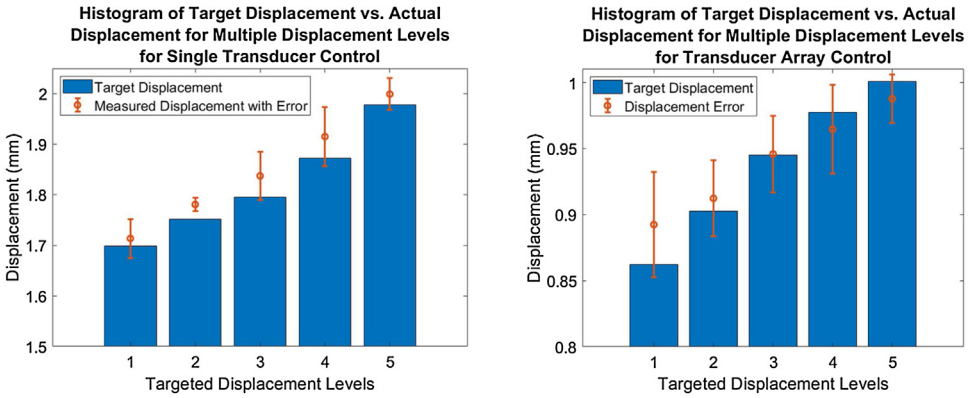


**Fig. 5.** A comparison of target displacement versus measured displacement for the single transducer and transducer array. Displacement was measured indirectly, by directly measuring the capacitance change and calculating displacement through Eq. 2. 50 trials were run with a variety of loading and target displacement conditions. The results were grouped by target displacement level to determine whether the error was a function of the amplitude. The range of displacement levels was chosen based on what was achievable for the used combinations of load and voltage. A) Single transducer. B) Transducer array.

actual displacement-capacitance relationships. To calculate a new voltage to reach a target displacement, a relationship between the measured capacitance and the displacement must be established. In this study, we have used a simple parallel plate capacitor as an approximation. It may be that this approximation holds for larger transducers, but is not as accurate for the smaller transducers that the array is composed of. A more complex equation which takes the complex geometry of the transducer electrodes into account may reduce this error. The relative variance was also significantly higher for the transducer array, which is hypothesized to be due to the previously-discussed reduced measurement sensitivity of the transducer array.

## 5. Conclusion

We demonstrated a flexible electrostatic transducer with controllable sensing and actuation. The transducer itself is lightweight and robust, yet capable of displacing loads up to 3 g. We built a custom electronics setup to precisely measure loads placed on the transducer and to maintain a average displacement for a range of loads. We were able to measure loads to within 2% and maintain displacement within 15 % of the chosen value. These loads are more than enough to be perceptible on the skin. A displacement amplitude an error of 15 % is barely detectable by a human user because the human vibrotactile amplitude discrimination threshold is on the order of 1–2 dB [24]. Significant reductions to these error values are expected for transducers fabricated using commercial methods, such as lithography. Current error is mostly caused by imperfections in the buckled film geometry, such that a given change in displacement does not map exactly to a set value of capacitance change. As the transducer is reduced in size and optimized for wearable applications, these values will correlate much more strongly.

This study also does not take into account the effect of parasitic capacitances from the body and environment. As the current capacitance ranges of the transducer are small, measurements are vulnerable to error due to changes in parasitic capacitance. In laboratory conditions, the absolute magnitude of parasitic capacitance is not relevant, as only changes in capacitance are used for measurements. In real-world use, the amount of parasitic capacitance would vary dynamically with device orientation and use. When the transducer is only sensing as a method of displacement control, this issue can be solved by extracting the amplitude change at the driving frequency only, but reducing the effect of parasitic capacitance for the case of general force and displacement sensing will require more sophisticated sensing electronics.

In addition, all of these experiments took place at driving voltages of at most 300 V, showing that the technology could be integrated into a small wearable device. Better fabrication methods will also allow the thickness of the insulator between the electrodes to be reduced, driving down the required voltage to levels easily attainable by safe consumer-oriented integrated circuits. The transducer matrix further shows the potential of the technology to be miniaturized and integrated. We demonstrated that the same sensing and actuating technologies that drive the single transducer are also effective at driving a matrix of smaller transducers. As the number of transducers in the matrix is increased, and the size of the individual transducer elements is decreased, the sensing spatial resolution and accuracy should increase dramatically. This matrix is similar to what could be actually used in commercial devices and shows the promise of this new flexible transducer technology.

## CRediT authorship contribution statement

**Ian Trase:** Conceptualization, Formal analysis, Investigation, Methodology, Software, Visualization, Writing - original draft, Writing - review & editing. **Hong Z. Tan:** Conceptualization, Formal analysis, Methodology, Writing - review & editing. **Zi Chen:** Conceptualization, Methodology, Writing - review & editing. **John X.J. Zhang:** Conceptualization, Methodology, Project administration, Supervision, Writing - review & editing.

## Declaration of Competing Interest

The authors have no competing interests to declare.

## Acknowledgements

The authors are grateful for the financial support of the National Science Foundation award (ECCS1509369), the National Institute of Health (NIH) Director's Transformative Research Award (R01HL137157), the Thayer School of Engineering PhD Innovation Program, and Facebook, Inc. under the SARA program. Z.C. acknowledges the support from the Branco Weiss–Society in Science Fellowship, administered by ETH Zürich.

## References

[1] G.M. Sessler, J.E. West, Electret transducers: a review, J. Acoust. Soc. Am. 53 (1973) 1589–1600, http://dx.doi.org/10.1121/1.1913507.
[2] T. Carter, S.A. Seah, B. Long, B. Drinkwater, S. Subramanian, UltraHaptics: multi-point mid-air haptic feedback for touch surfaces, UIST 2013 - Proc.26th

Annu. ACM Symp. User Interface Softw. Technol. (2013) 505–514, http://dx.doi.org/10.1145/2501988.2502018.
[3] F. Casset, J.S. Danel, C. Chappaz, Y. Civet, M. Amberg, M. Gorisse, C. Dieppedale, G. Le Rhun, S. Basrour, P. Renaux, E. Defay, A. Devos, B. Semail, P. Ancey, S. Fanget, Low voltage actuated plate for haptic applications with PZT thin-film, 2013 Transducers Eurosensors XXVII 17th Int. Conf. Solid-State Sensors, Actuators Microsystems, TRANSDUCERS EUROSENSORS 2013 (2013) 2733–2736, http://dx.doi.org/10.1109/Transducers.2013.6627371.
[4] S.B. Jung, S.W. Kim, Improvement of scanning accuracy of PZT piezoelectric actuators by feed-forward model-reference control, Precis. Eng. 16 (1994) 49–55, http://dx.doi.org/10.1016/0141-6359(94)90018-3.
[5] W. McMahan, K.J. Kuchenbecker, Dynamic modeling and control of voice-coil actuators for high-fidelity display of haptic vibrations, IEEE Haptics Symp. (2014) 115–122, http://dx.doi.org/10.1109/HAPTICS.2014.6775442.
[6] Y. De Chen, C.C. Fuh, P.C. Tung, Application of voice coil motors in active dynamic vibration absorbers, IEEE Trans. Magn. 41 (2005) 1149–1154, http://dx.doi.org/10.1109/TMAG.2004.843329.
[7] A. Dogan, Q. Xu, K. Onitsuka, S. Yoshikawa, K. Uchino, R.E. Newnham, High displacement ceramic metal composite actuators (Moonies), Ferroelectrics 156 (1994) 1–6, http://dx.doi.org/10.1080/00150199408215918.
[8] E.D. Burnham-Fay, T. Le, J.A. Tarbutton, J.D. Ellis, Strain characteristics of additive manufactured polyvinylidene fluoride (PVDF) actuators, Sens. Actuators A Phys. 266 (2017) 85–92, http://dx.doi.org/10.1016/j.sna.2017.08.053.
[9] Y. Roh, V.V. Varadan, V.K. Varadan, Characterization of all the elastic, dielectric, and piezoelectric constants of uniaxially oriented poled PVDF films, IEEE Trans. Ultrason. Ferroelectr. Freq. Control 49 (2002) 836–847, http://dx.doi.org/10.1109/TUFFC.2002.1009344.
[10] Z. Ma, D. Edge, L. Findlater, H.Z. Tan, Haptic keyclick feedback improves typing speed and reduces typing errors on a flat keyboard, in: IEEE World Haptics Conf, WHC 2015, 2015, pp. 220–227, http://dx.doi.org/10.1109/WHC.2015.7177717.
[11] I. Trase, Z. Xu, Z. Chen, H. Tan, J.X.J. Zhang, Thin-film bidirectional transducers for haptic wearables, Sensors Actuators A Phys. (2019), 111655, http://dx.doi.org/10.1016/J.SNA.2019.111655.
[12] I.H. Trase, Z. Xu, Z. Chen, H.Z. Tan, J.X.J. Zhang, Flexible electrostatic transducers for wearable haptic communication, Proc. World Haptics Conf. 2019 (2019), p. submitted.
[13] A. Villoslada, A. Flores, D. Copaci, D. Blanco, L. Moreno, High-displacement flexible shape Memory Alloy actuator for soft wearable robots, Rob. Auton. Syst. 73 (2015) 91–101, http://dx.doi.org/10.1016/j.robot.2014.09.026.
[14] C. Zheng, S. Shatara, X. Tan, Modeling of robotic fish propelled by an ionic polymer-metal composite caudal fin, Proc. SPIE - Int. Soc. Opt. Eng. 7287 (2009) 689–694, http://dx.doi.org/10.1117/12.815789.
[15] C. Keplinger, J.-Y. Sun, C.C. Foo, P. Rothemund, G.M. Whitesides, Z. Suo, Strctors, Science 341 (80) (2013) 984–987, http://dx.doi.org/10.1126/science.1240228.
[16] M. Matysek, P. Lotz, T. Winterstein, H.F. Schlaak, Dielectric elastomer actuators for tactile displays, in: Proc. - 3rd Jt. EuroHaptics Conf. Symp. Haptic Interfaces Virtual Environ. Teleoperator Syst, World Haptics 2009, 2009, pp. 290–295, http://dx.doi.org/10.1109/WHC.2009.4810822.
[17] D.J. Bell, T.J. Lu, N.A. Fleck, S.M. Spearing, MEMS actuators and sensors: observations on their performance and selection for purpose, J. Micromech. Microeng. 15 (2005), http://dx.doi.org/10.1088/0960-1317/15/7/022.
[18] R. Legtenberg, J. Gilbert, S.D. Senturia, M. Elwenspoek, Electrostatic curved electrode actuators, J. Microelectromech. Syst. 6 (1997) 257–265, http://dx.doi.org/10.1109/84.623115.
[19] A. Hajati, D. Latev, D. Gardner, A. Hajati, D. Imai, M. Torrey, M. Schoeppler, Three-dimensional micro electromechanical system piezoelectric ultrasound transducer, Appl. Phys. Lett. 101 (2012), http://dx.doi.org/10.1063/1.4772469.
[20] S. Rosset, B.M. O'Brien, T. Gisby, D. Xu, H.R. Shea, I.A. Anderson, Self-sensing dielectric elastomer actuators in closed-loop operation, Smart Mater. Struct. 22 (2013), http://dx.doi.org/10.1088/0964-1726/22/10/104018.
[21] J.J. Dosch, D.J. Inman, E. Garcia, A Self-Sensing Piezoelectric Actuator for Collocated Control, J. Intell, Mater. Syst. Struct. 3 (1992) 166–185, http://dx.doi.org/10.1177/1045389X9200300109.
[22] A. Punning, M. Kruusmaa, A. Aabloo, A self-sensing ion conducting polymer metal composite (IPMC) actuator, Sens. Actuators A Phys. 136 (2007) 656–664, http://dx.doi.org/10.1016/j.sna.2006.12.008.
[23] I. Trase, Z. Xu, Z. Chen, H. Tan, J.X.J. Zhang, Thin-film bidirectional transducers for haptic wearables, Sens. Actuators A Phys. (2019), 111655, http://dx.doi.org/10.1016/j.sna.2019.111655.
[24] R.T. Verrillo, G.A. Gescheider, Perception via the sense of touch, in: S. I (Ed.), Tactile Aids Hear. Impair, Whurr Publishers, London, 1992, pp. 1–36.

## Biographies

**Ian Trase** received his Bachelor's degree in Mechanical Engineering from Princeton University in 2014 with certificates in Materials Science and Engineering Physics. Ian's research experiences include internships at the Princeton Electric Propulsion Laboratory and MIT CSAIL. He is currently a pH.D. Innovation Fellow at the Thayer School of Engineering at Dartmouth, where his research focuses on flexible electronics and wearable haptics with an interest in translating technologies out of the lab to commercial applications.

**Hong Z. Tan** received her Bachelor's degree in Biomedical Engineering from Shanghai Jiao Tong University and earned her Master and Doctorate degrees, both in Electrical Engineering and Computer Science, from the Massachusetts Institute of Technology (MIT). She was a Research Scientist at the MIT Media Lab from before joining the faculty at Purdue University in 1998. She is currently a professor of Electrical and Computer Engineering, with courtesy appointments in the School of Mechanical Engineering and the Department of Psychological Sciences at Purdue University. Her research focuses on haptic human-machine interfaces, taking a perception-based approach to solving engineering problems.

**Dr. Zi Chen** is an Assistant Professor at Thayer School of Engineering at Dartmouth, an Adjunct Assistant Professor in the Department of Biological Sciences, and a PI at Dartmouth's Norris Cotton Cancer Center. He received his bachelor's and master's degree in Materials Science and Engineering from Shanghai Jiaotong University, and a PhD in Mechanical and Aerospace Engineering from Princeton University. Dr. Chen's research has been supported by NIH, Society in Science, and American Academy of Mechanics, and he has received the Society in Science-Branco Weiss Fellowship. He has published over 50 peer reviewed journal papers and filed two US patents.

**John X.J. Zhang** is a Professor at Thayer School of Engineering, Dartmouth College, and an Investigator of Dartmouth-Hitchcock Medical Center. He received his pH.D. from Stanford University, and was a Research Scientist at Massachusetts Institute of Technology. Dr. Zhang is a Fellow of American Institute for Medical and Biological Engineering, and a recipient of NIH Director's Transformative Research Award, NSF CAREER Award, DARPA Young Faculty Award, Facebook SARA award and many other recognitions. Zhang's research focuses on exploring bio-inspired nanomaterials, scale-dependent biophysics, and nanofabrication technology, towards developing new diagnostic devices, implantable bioenergy harvesting systems and wearable soft transducers.